IOP PUBLISHING JOURNAL OF MICROMECHANICS AND MICROENGINEERING

J. Micromech. Microeng. **18** (2008) 025027 (8pp) doi:10.1088/0960-1317/18/2/025027

Observation and optical implications of oil dewetting patterns in electrowetting displays

Bo Sun and Jason Heikenfeld

Novel Devices Laboratory, Department of Electrical and Computer Engineering, University of Cincinnati, Cincinnati, OH 45221, USA

E-mail: heikenjc@email.uc.edu

Received 3 October 2007, in final form 4 December 2007
Published 9 January 2008
Online at stacks.iop.org/JMM/18/025027

Abstract

Growth of surface instabilities leading to periodic oil patterns in electrowetting display pixels has been experimentally observed. In the electrowetting display pixels, an electrical potential ranging between 0 V and 80 V is applied among a water electrode, dielectric layers consisting of an oil film, fluoropolymer, Parylene C and a lower electrode. As predicted by spinodal dewetting theory, application of electromechanical pressure to the oil film causes the film to dewet into a periodic arrangement of oil droplets. The separation distance, or wavelength, for the dewetted oil droplets decreases with increasing voltage or with decreasing oil film thickness. Various test voltages of 20–80 V and oil thicknesses values of 3.3–8.9 μm were shown to experimentally generate dewetting wavelengths ranging from 10's to 100's of μm. An increased number of oil droplets inside the display pixel decreases the maximum display transmission or reflection proportional to the cube root of the number of droplets. This work therefore provides a means to further understand oil film dewetting in electrowetting display pixels and explains the implications of the dewetting pattern on display optical performance.

M This article features online multimedia enhancements

(Some figures in this article are in colour only in the electronic version)

Introduction

A recent explosion of growth in electrowetting research[1] is partially driven by a wide range of applications including lab-on-chip [1, 2], liquid lenses and prisms [3–5] and high-brightness displays [6, 7]. Electrowetting is an electromechanical effect [8, 9] whereby the balance of interfacial surface tensions (mN m^{-1}) near the solid/liquid/ambient contact line is altered by an electromechanical force per unit length. For optical applications, most electrowetting devices utilize water or saline and an immiscible oil ambient in order to reduce the influences of gravity, vibration, hysteresis and evaporation [10]. Recent oil/water electrowetting investigations for lab-on-chip [11] or fundamental study [12] have witnessed that a rapidly advancing water contact line can entrap a thin film of oil underneath the electrowetted water. It has been further shown that this oil film will exhibit a periodic break up into a pattern of oil droplets, and that the droplet spacing can be predicted by the fastest growing surface wavelength [12, 13]. This periodic oil dewetting can be referred to as form of spinodal dewetting that is dominated by electrostatic forces (not intermolecular van der Waals forces) [13]. Of the many applications for electrowetting, further examination of spinodal dewetting could be suggested as most important for display devices. In electrowetting displays, an electrostatically induced breakup of a colored oil film is utilized to alter the perceived coloration of a reflective or transmissive pixel. Early investigations of electrowetting displays [14, 15] have primarily dealt with oil initially resting in a spherical cap geometry, and thus the largest possible surface wavelength

[1] Electrowetting related patents and publications have grown at an annual rate of ∼70% since 2001 (source: data compiled by J Feenstra, LiquaVista Inc., 2007).

 © 2008 IOP Publishing Ltd Printed in the UK

was predetermined. More recently for these displays, it has been reported that the oil/water meniscus inside the pixel can rest in a flat geometry at zero voltage [16]. For maximum display contrast ratio (minimum light leakage) a dominantly flat meniscus is required. Since the oil film is thin (μm's) and is initially flat, multiple surface wavelengths can be generated inside a single pixel. Therefore based on the magnitude of the applied voltage, the oil can dewet into one or as many as dozens of oil droplets. Increasing the applied voltage, increasing the pixel area or decreasing the initial oil thickness should increase the number of oil droplets generated. Since all droplets have the same contact angle regardless of size, the ensemble of multiple droplets occupies a larger area than if the droplets were to combine as a single large droplet. This reduces the maximum reflection or transmission of the display, and also therefore reduces the maximum display contrast ratio. These issues have not been previously addressed and careful selection of device geometry and voltage level is necessary for obtaining maximum optical performance in electrowetting displays. Reported here is observation of electrowetting display pixels with spinodal dewetting patterns. The experimental data support a simple equation that can be used by display practitioners to predict oil film breakup in electrowetting displays. Also, since methods to experimentally test spinodal dewetting theory are not commonplace, the structures described herein provide a versatile new tool that can be utilized to explore spinodal dewetting theory. A brief discussion of fabrication and experimental conditions is first provided. Next, experimental results for dewetting patterns are presented and compared to theoretical results. Conclusions are then made on the role of voltage application on the optical performance of an electrowetting display. Lastly, several techniques are suggested that allow use of a flat oil film and dewetting of the oil into only a few droplets for the highest possible display contrast.

Fabrication and testing

All device structures tested herein utilize a base structure similar to that shown in figure 1. This layered structure consists of a substrate, a transparent and electrically conducting In_2O_3:SnO_2 film of ~100 nm thickness, a hydrophobic dielectric comprising a stack of 1.5 μm Parylene C and 0.2 μm DuPont Teflon AF, a dodecane oil film, and an overlying water layer. A detailed report of fabrication procedures and materials sources for the devices tested herein is found elsewhere [16]. For testing of display pixels, a hydrophilic polymer grid was additionally provided onto the surface of the hydrophobic dielectric. The dodecane oil film was colored with 7 wt.% red or blue dye. Materials parameters such as surface tension, dielectric permittivity and film thickness are discussed in later sections. Experimental observations were performed by viewing the top of the devices with a CCD camera mounted on a microscope. All photographs were taken immediately after oil film breakup was complete. DC voltage was applied to the electrically conductive water layer with the In_2O_3:SnO_2 held at electrical ground. All voltages were applied as step functions between 0 V and final dc voltage level. The slew rate of the voltage source is >10 V/1 μs and the RC time constant of the electrical setup is significantly faster than the ~ms microfluidic response time of any of the dewetting experiments discussed herein.

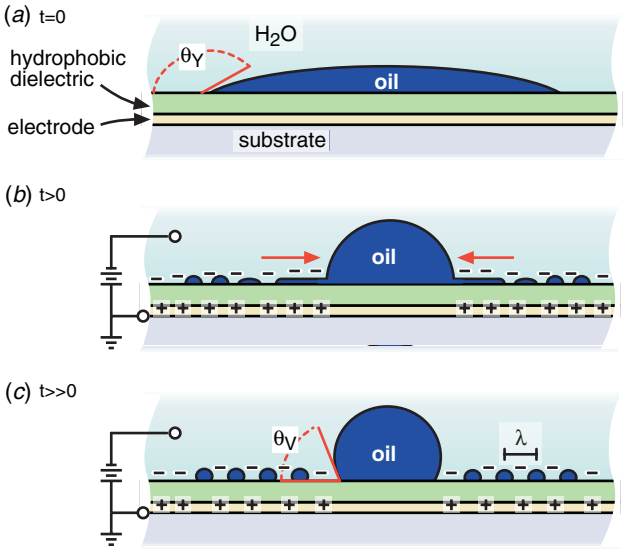


Figure 1. Diagram of electrowetting of a water/oil/hydrophobic–dielectric/electrode structure. Qualitative progression of the oil dewetting is shown in time lapse from (*a*) to (*b*) to (*c*). This dewetting scenario is representative of the case where the oil film initially has a spherical cap geometry in an electrowetting display pixel.

Electrowetting and spinodal dewetting for a spherical cap of oil

Electrowetting [10] involves application of voltage across a liquid/dielectric/electrode capacitor, a charge-induced imbalance of forces near the liquid/dielectric contact line and a resulting decrease in the macroscopically observed liquid contact angle. The macroscopically observed liquid contact angle can be predicted by the Young's equation and the so-called electrowetting equation

$$\gamma_{LD} = \gamma_{DA} - \gamma_{LA}\cos\theta_Y, \tag{1a}$$

$$\cos\theta_V = \cos\theta_Y + \frac{1}{2}\cdot\frac{\varepsilon\cdot V^2}{\gamma_{LA}\cdot d_{hyd}}, \tag{1b}$$

where θ_Y is Young's angle as determined by interfacial surface tensions (γ) at the three-phase conductive liquid (L), ambient (A), dielectric (D) contact line (figure 1(*a*)), d_{hyd} is the hydrophobic dielectric thickness, ε is the dielectric permittivity, ε/d_{hyd} is the dielectric capacitance per unit area (F m^{-2}) of the dielectric, V is the applied dc voltage or ac RMS voltage and θ_V is the macroscopically observed electrowetted contact angle (figure 1(*c*)). In this work, the liquid is deionized water and the ambient fluid is dodecane oil. These materials result in a Young's angle of ~170°. The electrowetting equation can be derived using



Figure 2. Photographs of electrowetting of a water/oil/hydrophobic-dielectric/electrode structure at (*a*) 0 V, (*b*) 0 V then 20 V applied and (*c*) 0 V then 40 V applied. The photographs are taken from a top view, and the oil layer is colored blue and spatially located similar to the diagrams in figure 1. A video clip of the spinodal dewetting process is provided in the on-line supplementary materials section of this paper available at stacks.iop.org/JMM/18/025027. This dewetting scenario is representative of the case where the oil film initially has a spherical cap geometry in an electrowetting display pixel.

energy minimization [17], interfacial thermodynamics [18] or electromechanics [8]. However, a recent study by Mugele [9] has further confirmed that the electromechanical approach developed by Jones [8] is fundamentally the most complete approach. For an electrowetted droplet, Mugele provided supporting theory and direct observation that the microscopic contact angle remains unchanged (i.e. Young's) even as the droplet is macroscopically observed to decrease in contact angle with increasing voltage. It has been further shown by Mugele that the advancing liquid contact line therefore results in entrapment of a thin oil film according to the Landau–Levich law of dip coating [12]. More important to this work, a flat thin oil film that is subject to an electromechanical pressure can become unstable. This should cause the oil film to exhibit a periodic breakup into droplets according to a process referred to as spinodal dewetting [13]. As shown diagrammatically in figures 1(*b*) and (*c*), and in the photographs of figure 2, spinodal dewetting of the oil films is readily achieved with the materials utilized herein. The blue area in figure 2 is the dye-colored oil, and the entire device is covered with water. A video clip of the electrowetting experiment shown in figure 2 is provided with the online supplementary information for this paper available at stacks.iop.org/JMM/18/025027. The periodicity of oil film breakup along a given circumference is visually obvious in figure 2. It can also be observed in figure 2 that an initial applied voltage of 40 V results in smaller and more closely spaced droplets than the case for 20 V. This decrease in the period between droplets with increase in voltage follows the general behavior expected by spinodal dewetting theory [12], which will be discussed in greater detail in the following sections. The devices of figures 1 and 2 are presented herein because they are representative of how spinodal dewetting can manifest in electrowetting pixels where the oil has a spherical cap geometry at 0 V [14, 15]. The primary focus of the work, as presented in the following sections, will deal with higher contrast display pixels where the oil initially has a flat film geometry at 0 V [16].

Electrowetting and spinodal dewetting for a flat oil film

Attention is now turned to a theoretical prediction of spinodal dewetting for an oil film with a flat geometry at 0 V. Under electromechanical pressure the many possible dewetting modes for a flat oil film grow at differing exponential rates. During the dewetting, a single mode, or surface wavelength (λ), can dominate according to

$$\lambda = 2\pi/\nu, \tag{2a}$$

$$\nu^2 \cong \frac{A}{4\pi \cdot d_{\text{oil}}^4 \cdot \gamma_{\text{LA}}} + \frac{\varepsilon \cdot V^2}{2 \cdot d^3 \cdot \gamma_{\text{LA}}}, \tag{2b}$$

where ν is the wave number of the fastest growing oil film dewetting mode, A is the Hamaker constant for the oil film, V is the sum of applied voltage and the work function difference between the electrode and water, and d and ε are the total equivalent thickness and permittivity of the series capacitance of the oil film (d_{oil}, ε_{oil}) and hydrophobic dielectric (d_{hyd}, ε_{hyd}) [12, 13]. As described in detail by Herminghaus [13], for the materials and geometries tested herein the portion of equation (2*b*) with $\left[A/\left(4\pi \cdot d_{\text{oil}}^4 \cdot \gamma_{\text{LA}}\right)\right]$ can be neglected in calculating λ since the portion of equation (2*b*) with $\varepsilon \cdot V^2/(2 \cdot d^3 \cdot \gamma_{\text{LA}})$ dominates the dewetting (i.e. electromechanical forces far exceed intermolecular van der Waals forces) [13]. It should be further noted that equation (2*b*) is an approximated version of the equation presented by Mugele [12]. This approximated equation (2*b*) is utilized since it eases the readers interpretation of the data trends. This is allowable since the oil film limits the oil/hydrophobic dielectric series capacitance in electrowetting displays [6, 14, 15]. To check the validity of this approximation, comparative calculations were made for the thinnest oil layer tested herein. The maximum difference in calculating λ was only ~7% as calculated by comparing Mugele's equation [12] to equation (2) for the case of the thinnest oil layer ($d_{\text{oil}} = 3.3\ \mu$m). At this point it should be noted that this thinnest oil layer tested is at the limit of what

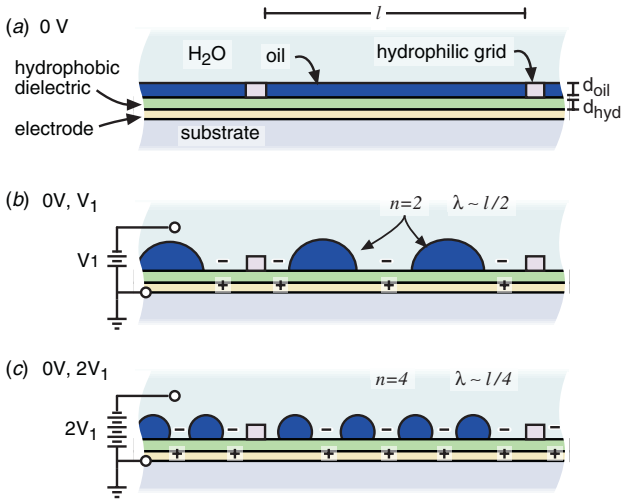


Figure 3. Diagram of a water/oil/hydrophobic-dielectric/electrode electrowetting display structure (*a*). Qualitative representation of the oil dewetting for (*b*) a first voltage and (*c*) twice the magnitude of the first voltage is provided along with marking of how the fastest growing wavelength (λ) is calculated.

is needed for the oil film to exhibit proper color saturation for display applications. Therefore, the approximated equation (2*b*) is universally valid for electrowetting displays. Non-ideal electrowetting effects [10] such as charge injection, contact angle saturation or contact angle hysteresis should not play any role in the spinodal dewetting process since wavelength selection occurs nearly instantaneously (i.e. well before the water reaches the hydrophobic dielectric layer).

Description of electrowetting pixel structures tested

Next discussed is the experimental device structure specific to this work: an electrowetting display pixel where the flat oil film is horizontally bound by a hydrophilic grid. Operation of the display pixels is diagramed in figure 3 and differs from simple droplet electrowetting due to the addition of a hydrophilic grid. The hydrophilic grid defines the perimeter of the individual display pixels. As shown in figure 3, application of voltage causes dewetting of a colored oil film. For display applications, when the colored oil film is broken up the visual appearance of the pixel is changed from uniform color (oil film) to the color provided behind the pixels [6]. The coloration behind the pixels is most often a white reflective film or a backlight unit (not shown in figure 3). When the voltage is removed, interfacial surface tension forces cause the oil to recover the surface in a flat film geometry. Full reversibility over multiple switching cycles was observed for the electrowetting pixels tested herein. For the display pixels tested it has been previously shown that the oil film in each cell can be dosed via self-assembly with a uniform oil thickness (d_{oil}) that is equal to the hydrophilic grid height [16]. Previous theoretical investigations of electrowetting pixels [14, 15] have primarily involved pixel structures with a spherical cap oil geometry at 0 V, and therefore, a predetermined dewetting geometry in the form of a single drop (i.e. the largest possible wavelength). The flat geometry of the pixels tested herein does not have this predisposition to any particular wavelength for the oil dewetting. Defects, particulates, and the influence of the sidewall of the hydrophilic grid may play some role in wavelength selection, but as will be seen in the experimentally measured data, the wavelength selection is clearly dominated by the parameters of oil film thickness and applied voltage in equation (2). Furthermore, in this work all experimental materials parameters relevant to equation (2) are known. Therefore, in this work, wavelength selection predicted by equation (2) can be directly compared to the experimental observations. Device fabrication was performed similar to that reported previously [16]. Important materials and testing parameters include the following. Applied voltages to the water include a negative polarity voltage of 0 V, 10 V, 20 V, 40 V, 60 V, 80 V. Oil film thicknesses (d_{oil}) tested include 3.3 μm, 4.7 μm, 6.7 μm and 8.9 μm, and the oil film permittivity is $\varepsilon \sim 2\varepsilon_0$. The hydrophobic dielectric comprised a lower layer of 1.5 μm of Parylene C with $\varepsilon \sim 3\varepsilon_0$, and a top coating of 0.2 μm of Teflon AF with $\varepsilon \sim 2\varepsilon_0$. The 7 wt.% of dye colorant added to the dodecane reduces γ_{LA} from ~50 mN m^{-1} for dodecane/water to a value of ~30 mN m^{-1} for dodecane:dye/water. Pixels sizes are determined by the hydrophilic grid spacing and pixels sizes tested herein are 50 × 150 μm^2, 100 × 300 μm^2, 200 × 600 μm^2 and 300 × 900 μm^2. The hydrophilic grid is formed from SU-8 epoxy and promotes a flat oil meniscus since the sidewalls of the SU-8 exhibit a water/oil contact angle of ~90° [16]. Using the materials parameters defined above, equation (2) can be further simplified to theoretically predict the fastest growing wavelength according to $\lambda \approx 346.5 \times d^{3/2}/V$ (μm), where as previously stated d includes both d_{hyd} and d_{oil}, and is inserted in units of μm.

Experimental results and interpretation

Experimentally observed wavelength calculation was performed as follows. As shown in figure 3, the dewetting wavelength was calculated by summing the number of oil droplets (n) along the length of the pixel (l) and dividing the pixel length (l) by the number of droplets (n) to achieve the wavelength according to ($\lambda \approx l/n$). It should be noted that the oil has two-dimensional freedom in dewetting, but the sidewalls for each pixel place further restrictions on Herminghaus's theoretical equation (equation (2)) derived for an oil film without horizontal boundary [13]. Said differently, the rigid pixel sidewall creates a boundary condition that could favor the appearance of discrete wavelengths. However, if multiple wavelength periods are generated within the pixel, the error associated with discrete modes will not be distractive from the main conclusions of this work. To further improve accuracy, multiple pixels were measured for each pixel length (l) and oil thickness (d_{oil}). All collected data were found to be repeatable across multiple display prototypes and multiple voltage cycles. It will next be seen that despite the presence of pixel sidewalls, the above-described method for calculating dewetting wavelength allows very good agreement between equation (2) and the experimental data. However, the authors

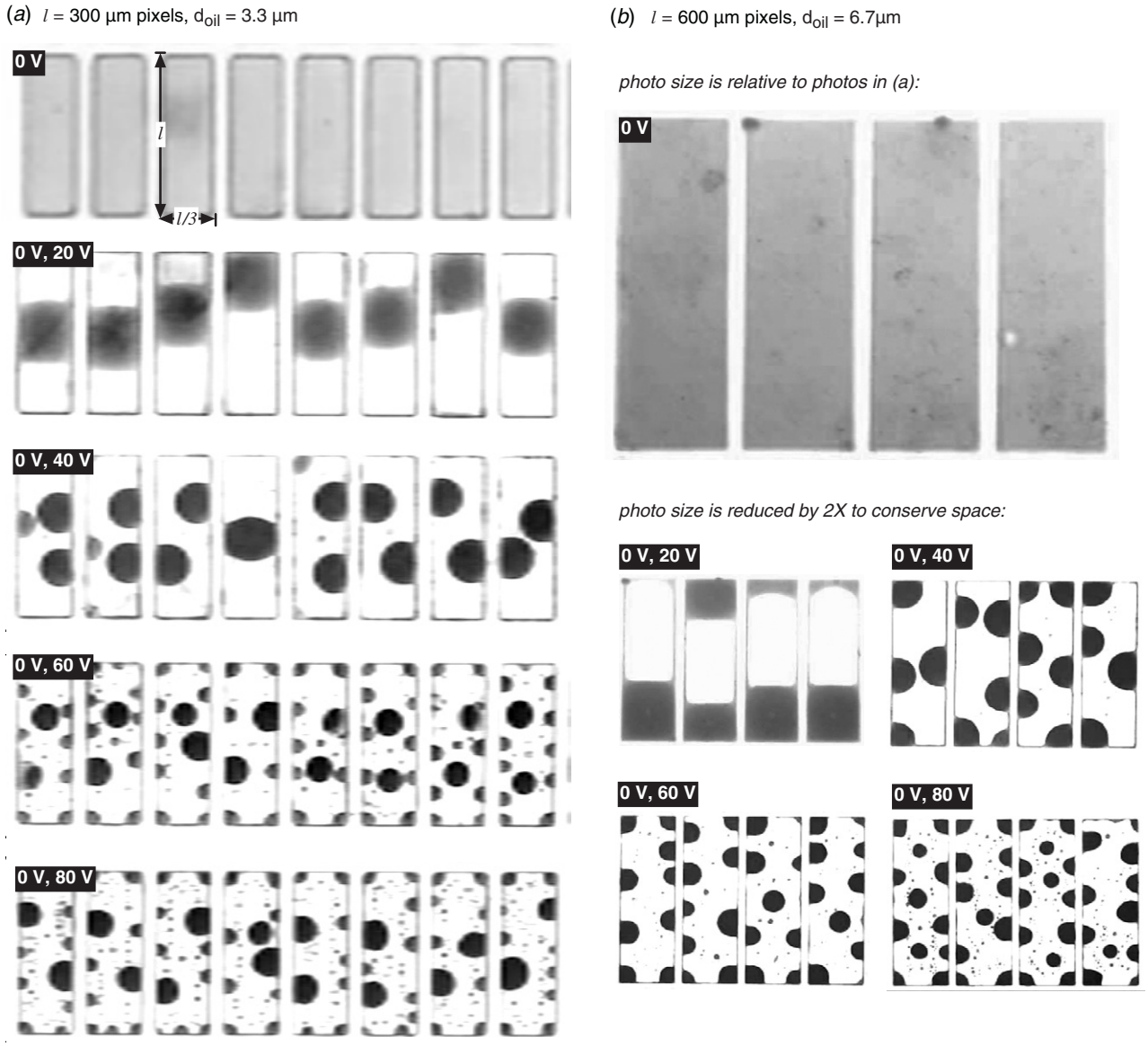


Figure 4. Photographs of (*a*) 100 × 300 μm^2 pixels with 3.3 μm thick oil and (*b*) 200 × 600 μm^2 pixels with 6.7 μm thick oil. The photographs include an oil film that is initially at rest and having a flat geometry inside the pixel (0 V), and for dewetted oil films after a variety of voltage levels were applied. The clear space between the pixels is the hydrophilic grid. In (*b*) the photograph size at 0 V is first shown at relative size to the photographs in (*a*), and the remainder of photographs in (*b*) are relatively reduced 2× to conserve space. A video clip of spinodal dewetting in an electrowetting pixel is provided in the on-line supplementary materials section of this paper available at stacks.iop.org/JMM/18/025027.

caution that it is *not* the objective of this work to prove that equation (2*b*) is the most complete formula for predicting the spinodal dewetting *wavelength* in display pixels. Rather, the important conclusions that will be made are: (1) the oil dewetting is periodic and predictable; (2) the dewetting follows the general principles of spinodal dewetting with variation of the parameters for dielectric thickness (*d*) and applied voltage (*V*); (3) the dewetting pattern has important implications on the operation and optical performance of an electrowetting display pixel.

Further attention on the experimental observations is now provided. As diagramed in figures 3(*b*) and (*c*), for larger applied voltages, an increased number of droplets should be observed. This is clearly the trend as seen in the photographs of figure 4. For figure 4(*a*), d_{oil} is 3.3 μm and pixel size is 100 × 300 μm^2. For figure 4(*b*), d_{oil} is 6.7 μm and pixel size is 200 × 600 μm^2. In the photographs, higher applied voltage (*V*) results in increased number of droplets (*n*) along a sidewall, decreased associated wavelength (λ) and decreased droplet size. Also, the oil for the devices in figure 4(*b*) is thicker than that for figure 4(*a*), and as expected the thicker oil (larger *d*) has the opposite effect of increased voltage (i.e. larger droplets, less droplets and larger dewetting wavelength). It should also be noted that droplets most often

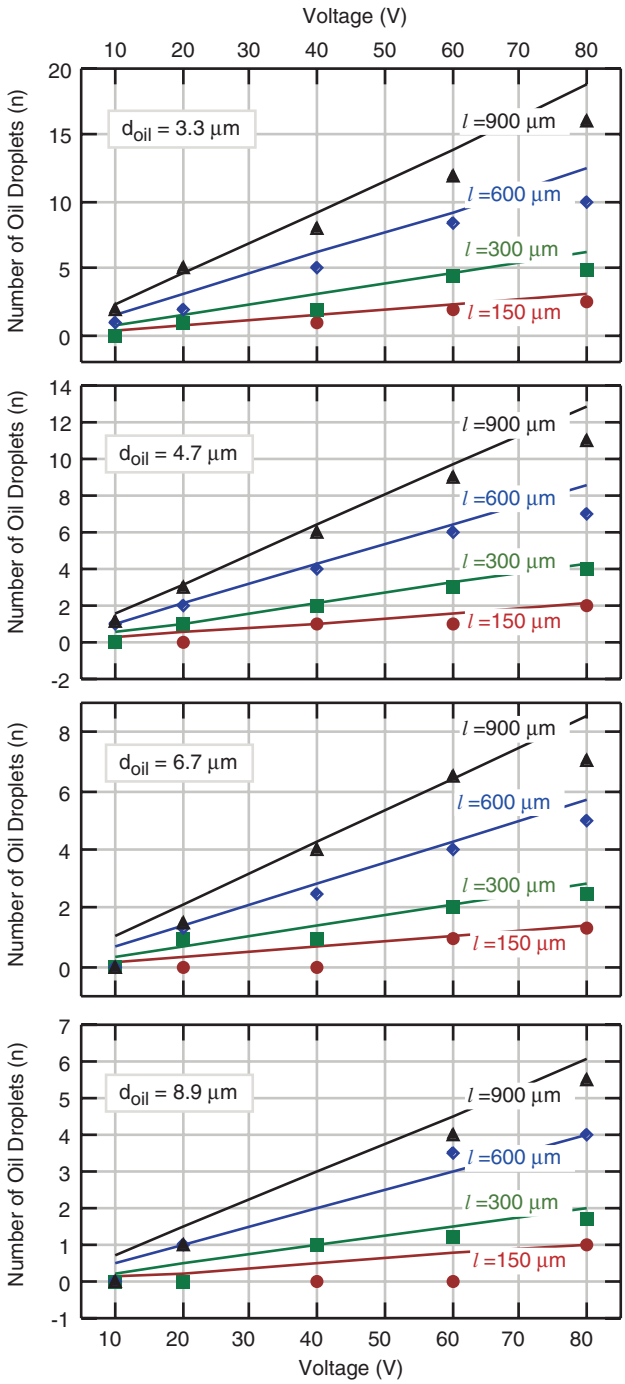


Figure 5. Plots of the average number of oil droplets (n) counted along the pixel sidewall versus applied voltage for various pixel sizes (l) and oil film thicknesses (d_{oil}). The solid lines represent the theoretically predicted response using equation (2). The experimental data are shown as dots. For maximum accuracy, all tested display structures were fabricated in parallel. The few missing data points simply represent fabrication failures.

situate adjacent to the sidewalls and corners, suggesting that pixel sidewalls do create discrete modes for the dewetting. The average droplet counting data collected for all pixels sizes, oil thicknesses and voltage levels are summarized in

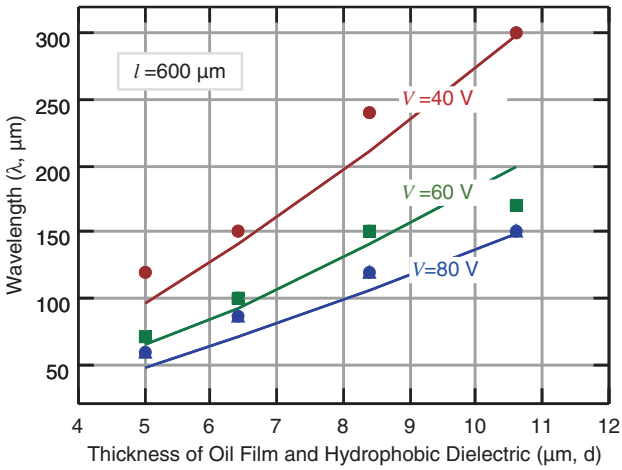


Figure 6. Plots of the fastest growing wavelength versus dielectric thickness. The dielectric thickness (d) is the sum of the thicknesses for the hydrophobic dielectric layer and the oil film. The solid lines represent the theoretically predicted response with the materials parameters used in the experiments. The experimental data are shown as dots.

the plots of figure 5. In figure 5, the solid lines represent the theoretical behavior predicted by equation (2). In agreement with equation (2), the droplet counts plotted in figure 5 increase linearly with increasing applied voltage. The data have also been plotted in figure 6 as the fastest growing wavelength ($\lambda \approx l/n$) versus the sum of the oil and hydrophobic dielectric thicknesses (d). The experimental data support that λ has a $d^{3/2}$ dependence and accordingly that electrostatic forces dominate over intermolecular forces in the spinodal dewetting process [12]. In figure 6, only the data for $l = 600\ \mu$m are shown since the other pixel lengths tested exhibited similar agreement. Therefore, the experimental data and plots in figures 4–6 all support that the oil dewetting process is spinodal in nature. The data also support that the further simplified version of equation (2), $\lambda \approx 346.5 \times d^{3/2}/V\ (\mu\text{m})$, is a useful tool for predicting oil film breakup as a function of both voltage and oil thickness. Other interesting observables and discussion can be made upon the results reported herein. Such items of further interest can be found in the appendix and the second online supplemental video for this paper available at stacks.iop.org/JMM/18/025027. With the main observable of predictable dewetting patterns now in hand, attention is next turned to practical implications on display performance.

Implications on display performance

Now that it is shown that the oil dewetting is periodic and predictable as a function of voltage and oil thickness, attention may be turned to implications of this work on the optical performance of electrowetting displays. In previous generations of electrowetting display devices, the pixel sizes were large (~mm) and the oil films thick (~10's μm) [6, 19]. Larger pixel sizes require less voltage to initiate the dewetting [16]. Therefore, these early generations of electrowetting devices exhibited dewetting of the oil into one or two droplets

of oil. However, to meet commercial display requirements, electrowetting pixels are now scaled down to pixel sizes on the order of ~100 μm (10× smaller). In order to maintain a constant voltage requirement ($V < 15$ V), as the pixel size (l) is decreased the combined thickness of the oil and the hydrophobic dielectric is typically decreased to $d \sim 5$ μm [16]. For such thin oil films, in order to maintain proper color saturation the wt.% of dye is increased to near its maximum level [19]. These thin oil films typical to commercial scale electrowetting displays are therefore subject to dewetting into multiple oil droplets (n). Multiple oil droplets reduce the optical performance of the display since for a reflective mode [6] or transmissive mode display [20] the white-state brightness is maximized when the oil area inside the pixel is minimized. Assuming display operation where the pixel ON state involves electrowetting to $\theta_V = 90^\circ$, the cumulative area occupied by all oil droplets inside a single pixel is proportional to cube root of the number of oil droplets ($n^{1/3}$). If oil film breakup provides a single droplet ($n = 1$) that occupies 20% of the pixel area, then for multiple droplets the oil area will be ($n = 2$, 25%), ($n = 4$, 32%), ($n = 8$, 40% of the pixel area), etc. It is therefore clear that the optical performance of the display is strongly dependent on the droplet count in each pixel. Some brief speculation is next provided on how the effects of droplet count may be mitigated. First, one should recall that for minimum optical transmission in the pixel OFF state, the colored oil film should be geometrically flat to eliminate unwanted transmission at thinner sections of oil [16]. To promote a single droplet formation with a dominantly flat oil geometry, a small area of one corner of the pixel may be made hydrophilic to provide a predetermined dewetting wavelength. This technique has been previously demonstrated [20]. In an alternate technique to promote single droplet formation, a slow voltage ramp could be utilized. However, a ramped voltage will reduce the maximum allowable display refresh rate. Therefore, a two-step voltage may be preferred for reducing the droplet count. Using a two-step voltage, the first lower voltage level would start the growth of a wavelength (λ) comparable to the pixel size (l). The second higher voltage level would then be applied and would drive the system to a minimum water contact angle. This would provide minimum oil area inside the pixel and maximum optical contrast. It is interesting to point out that according to the Beer–Lambert law, multiple droplets will individually have a larger optical transmission at their center than a larger and thicker droplet. Therefore, there could be intermediate levels of oil opacity and pixel geometries that would provide higher maximum transmission or reflection for the case of multiple oil droplets. However, such pixels would not provide the highest possible ON/OFF contrast ratios for display applications, and such optical theory is beyond the scope of this work.

There is another topic related to display performance that is worthy of brief discussion. As previously reported [16], the voltage required to start the dewetting of the oil decreases as the pixel size is increased. Examining the pixels at the threshold voltage for dewetting, it was observed for all pixel sizes and oil thickness tested herein that the voltage required to start the dewetting process is sufficiently low for the formation of a single oil droplet (i.e. the largest possible wavelength). At first glance, one might be tempted to correlate the threshold voltage for oil film breakup with creation of the first allowed dewetting mode (i.e the largest wavelength). However, the authors make note that since all wavelengths are allowed at any given voltage, the existence of threshold voltage for dewetting should *not* be correlated with appearance of the first wavelength. This is because at any given voltage, pixel size or oil film thickness, all wavelengths are allowed to form, but according to spinodal dewetting theory one wavelength simply grows the fastest and dominates. The threshold voltage for oil film break up is related to the threshold at which electromechanical forces exceed surface tension forces. The observation in the present work that the threshold voltage produces the largest wavelength is simply a coincidence of the specific device geometries and materials tested herein.

Summary

In summary, growth of surface instabilities leading to periodic oil patterns in electrowetting display pixels has been experimentally observed. A variety of pixel geometries have been demonstrated and show that the oil dewetting is periodic and predictable. It has been further shown that the dewetting follows the general principles of spinodal dewetting with variation of the parameters for dielectric thickness and applied voltage. The practical implication of these findings is that the optical performance of an electrowetting display will degrade if multiple droplets are produced inside a single electrowetting pixel. This work also provides an additional investigative tool that researchers might utilize to experimentally explore spinodal dewetting across a wide range of materials and electrical parameters.

Acknowledgments

Research support for electrowetting displays at Cincinnati includes K Zhou, Y Lao, and is gratefully acknowledged. The authors thank R Schwartz of Sun Chemical for input and encouragement on this work and acknowledge partial support of this work by an industrial research grant from Sun Chemical. The authors would also like to thank K Dean and E Howard of Motorola Labs for input and encouragement on this work and acknowledge partial support of this work through a Motorola Inc. University Partnership in Research award. Lastly, the authors would like to thank W Cheng and others at the Industrial Tech. Research Institute, Taiwan for their support in co-advancing electrowetting display technology with researchers at Cincinnati.

Appendix. Other important considerations and observables

Several other important considerations and observables are provided in this appendix. Rectangular pixels were examined because they are of the aspect ratio (3:1) typically used in displays. Measuring along the pixel length is further useful because the most wavelength periods (oil droplets) should

appear. This should reduce the effects of discrete wavelengths and increase the accuracy of the data collection. Although not included in the data, the above-described measurement approach also worked well for square pixels that were large enough ($>300 \times 300\ \mu m^2$) for multiple wavelengths to appear along the pixel sidewall. The presented rationale for calculating the wavelength is further supported by photographs of both figures 4(*a*) and (*b*). The oil film breakup and largest wavelength to appear at ~20 V is clearly along the length of the pixel. This first wavelength is too large to appear across the pixel width. In the photographs, not until higher voltages, and therefore smaller wavelengths, does the oil split across the width of the cell.

It should also be noted that at higher voltages very small droplets can be observed in the photographs. These small droplets were correctly ignored in the data collection and are due to oil film entrapment and a second manifestation of spinodal dewetting like that described for figures 1 and 2. As seen in the second online supplemental video provided with this paper, in some cases larger droplets along a sidewall can be counted as two droplets since they result from the coalescence of two smaller droplets (available at stacks.iop.org/JMM/18/025027). In some cases, it has been observed in the videos that a small capillary of oil remains at the sidewall edges and therefore causes smaller oil droplets (smaller radius of curvature, *r*) to flow into larger oil droplets (larger *r*) through the small capillary of oil. This droplet-to-droplet flow is driven by a differential Young–Laplace pressure ($2\ \gamma_{LA}/r$) between the droplets. Therefore, to ensure the counting of droplets is representative of only spinodal dewetting, the droplets were counted immediately after the occurrence of the oil film breakup (i.e. before coalescence could occur). Also, careful inspection of the second online video reveals that at higher voltages, most droplets experience an increase in area as the dc voltage is held. This should be explained as well, and is direct evidence of charge injection into the hydrophobic dielectric. Charge injection causes the water contact angle to increase (or 'relax') and the observation of a slight expansion of the oil coverage area [10].

References

[1] Pollack M G, Fair R B and Shenderov A D 2000 Electrowetting-based actuation of liquid droplets for microfluidic applications *Appl. Phys. Lett.* **77** 1725–26

[2] Moon H, Cho S K, Garrell R L and Kim C J 2002 Low voltage electrowetting-on-dielectric *J. Appl. Phys.* **92** 4080–7

[3] Berge B and Peseux J 2000 Variable focal lens controlled by an external voltage: an application of electrowetting *Eur. Phys. J.* E **3** 159–63

[4] Kuiper S and Hendriks B H W 2004 Variable-focus liquid lens for miniature cameras *Appl. Phys. Lett.* **85** 1128–30

[5] Smith N R, Abeysinghe D C, Haus J W and Heikenfeld J 2006 Agile wide-angle beam steering with electrowetting microprisms *J. Opt. Exp.* **14** 6557–63

[6] Hayes R A and Feenstra B J 2003 Video-speed electronic paper based on electrowetting *Nature* **425** 383–5

[7] Heikenfeld J and Steckl A J 2005 Intense switchable fluorescence in light wave coupled electrowetting devices *J. Appl. Phys. Lett.* **86** 011105

[8] Jones T B, Fowler J D, Chang Y S and Kim C J 2003 Frequency-based relationship of electrowetting and dielectrophoretic liquid microactuation *Langmuir* **19** 7646–51

[9] Mugele F and Buehrle J 2007 Equilibrium drop surface profiles in electric fields *J. Phys.: Condens. Matter* **19** 375112

[10] Mugele F and Baret J C 2005 Electrowetting: From basics to applications *J. Phys.: Condens. Matter* **17** R705–74

[11] Fair R B 2007 Digital microfluidics: is a true lab-on-a-chip possible? *Microfluid Nanofluid* **3** 245–81

[12] Staicu A and Mugele F 2006 Electrowetting-induced oil film entrapment and instability *Phys. Rev. Lett.* **97** 167801

[13] Herminghaus S 1999 Dynamical instability of thin liquid films between conducting media *Phys. Rev. Lett.* **83** 2359–61

[14] Roques-Carmes T, Hayes R A and Schlangen L J M 2004 A physical model describing the electro-optic behavior of switchable optical elements based on electrowetting *J. Appl. Phys.* **96** 6267–71

[15] Roques-Carmes T, Hayes R A, Feenstra B J and Schlangen L J M 2004 Liquid behavior inside a reflective display pixel based on electrowetting *J. Appl. Phys.* **95** 4389–96

[16] Sun B, Zhou K, Lao Y, Heikenfeld J and Cheng W 2007 Scalable fabrication of electrowetting displays with self-assembled oil dosing *Appl. Phys. Lett.* **91** 011106

[17] Berge B 1993 Electrocapillarity and wetting of insulator films by water *C. R. Acad. Sci., Paris II* **317** 157–63

[18] Welters W J J and Fokkink L G J 1998 Fast electrically switchable capillary effects *Langmuir* **14** 1535–8

[19] Roques-Carmes T, Palmier S, Hayes R A and Schlangen L J M 2005 The effect of the oil/water interfacial tension on electrowetting driven fluid motion *Colloid Surf.* A **267** 56–63

[20] Heikenfeld J and Steckl A J 2005 Electrowetting light valves with greater than 80% transmission, unlimited view angle, and video response *Proc. Soc. Inf. Disp.* P56.3